

Titanium-Oxide-Based Electron-Selective Contact for Ultrathin Germanium Quantum Well Solar Cell

Norbert Osterthun,* Hosni Meddeb, Dennis Berends, Nils Neugebohrn, Kai Gehrke, Martin Vehse, and Carsten Agert

In solar cells with an optical cavity as a light trapping mechanism, parasitic absorption is among the main detrimental optical losses. One approach to reducing these losses is the implementation of charge carrier-selective contacts with wide bandgaps using thin metal oxides like titanium oxide (TiO_x). Herein, it is proved that TiO_x is a suitable alternative for lossy *n*-doped hydrogenated amorphous silicon (*n* a-Si:H) as electron selective contact in ultrathin solar cells based on intrinsic hydrogenated amorphous germanium (a-Ge:H). The integration of the TiO_x layer leads to an improved photocurrent generation in the blue light wavelengths. Furthermore, a substantial extraction of charge carriers is demonstrated from the a-Ge:H quantum well nanoabsorber embedded between intrinsic a-Si barrier layers. However, the substitution of *n* a-Si:H by TiO_x results in limited photovoltaic performance due to a lower open-circuit voltage. This effect is analyzed via electrical simulation considering a variation in the electron affinity and the doping of TiO_x as well as the defect density in the silicon buffer. Moreover, the TiO_x -based solar cell exhibits improved light transmittance when the opaque back contact is omitted, which is beneficial for semi-transparent applications.

1. Introduction

Thin-film solar cells enable special semitransparent applications like photovoltaic solar windows^[1–4] or spectrally selective solar cells for greenhouses.^[4–6] A partial transmittance of visible light can be achieved by using wide-bandgap photoactive materials or by reducing the absorber thickness.

In this context, one possible design is the ultrathin amorphous germanium (a-Ge:H) nanoabsorber solar cell. This type of solar cell uses an optical resonant nanocavity for highly efficient light trapping.^[7–9] The incident light is confined into an ultrathin

a-Ge:H quantum well (QW) absorber due to constructive interference from nontrivial phase shifts at the interfaces between the semiconductor and the electrical contacts. Interestingly, the large Bohr radius of ≈ 24 nm for germanium enables quantum-size effects for absorber thicknesses below this range.^[8–11] This leads to a widening of the a-Ge:H quantum well bandgap of the nanoabsorber from 0.98 eV for 20 nm to 1.56 eV for 2 nm and allows a major increase in the open-circuit voltage and fill factor.^[8]

The photocurrent generation and the transmittance in a semitransparent configuration of this type of solar cell are limited by reflection losses and by parasitic absorption losses in the doped silicon layers. Due to the optical resonant nanocavity, multiple lights passing through the doped layers occur. This leads to parasitic absorption losses of up to 20% for blue light,^[5] since the doped silicon has a high absorption coefficient in

this wavelength range. One approach to overcome the absorption losses is to substitute the doped layers with high bandgap metal oxides as charge carrier-selective contacts.^[12–14] One of the most studied metal oxides in this context is titanium oxide (TiO_x).^[15–20] It is successfully applied in organic and dopant-free asymmetric hetero-contact (DASH) silicon solar cells. Due to different stoichiometries, TiO_x exhibits a wide range of work functions between 3.8 and 4.4 eV and doping levels between $1\text{E}16$ and $3\text{E}19\text{ cm}^{-3}$.^[19–21] Therefore, it can be used as electron or hole selective contact depending on criteria such as work function and doping level.^[15,16]


In this publication, we compare *n*-doped hydrogenated amorphous silicon (*n* a-Si:H) and TiO_x -based electron selective contacts for an a-Ge:H solar cell. We show that sputtered TiO_x is a suitable alternative for the *n* a-Si:H and that the transmittance of the solar cell without the opaque back contacts is significantly improved. However, after the implementation of TiO_x contacts, a decrease in V_{oc} was observed. We performed electrical simulations to determine the origin of the decrease and suggest possible solutions for a future enhancement of the cell performance.

2. Experimental Section

2.1. Solar Cell Fabrication and Characterization

The solar cell layer stacks were deposited on $10 \times 10\text{ cm}^2$ glass substrates with a 1000 nm thick aluminum doped zinc

N. Osterthun, H. Meddeb, D. Berends, N. Neugebohrn, K. Gehrke, M. Vehse, C. Agert
Urban and Residential Technologies
German Aerospace Centre (DLR) Institute of Networked Energy Systems
Carl-von-Ossietzky-Str. 15, Oldenburg 26129, Germany
E-mail: norbert.osterthun@dlr.de

 The ORCID identification number(s) for the author(s) of this article can be found under <https://doi.org/10.1002/pssa.202200292>.

© 2022 The Authors. physica status solidi (a) applications and materials science published by Wiley-VCH GmbH. This is an open access article under the terms of the Creative Commons Attribution License, which permits use, distribution and reproduction in any medium, provided the original work is properly cited.

DOI: 10.1002/pssa.202200292

oxide front contact (AZO, aluminum doping 0.5 wt%). A 7 nm thick TiO_x layer was deposited at $T_{\text{substrate}} = 200^\circ\text{C}$ via reactive magnetron sputtering. A titanium rotatable target was used and argon, as well as oxygen, were used as process gasses. The oxygen flow was continuously adjusted with a closed-loop partial pressure control, whereas the argon flow was kept constant. The detailed process parameters are summarized in **Table 1**. After ex situ transfer, the silicon and germanium functional layers were added via plasma-enhanced vapor deposition (PECVD). The detailed process parameters of the silicon and germanium functional layers can be found in a previous publication.^[4]

Furthermore, an a-Ge:H reference cell was prepared with an a-Si:H contact and an identical AZO front contact.^[8] Here, the functional layers were deposited via a PECVD process without a vacuum break. The deposition parameters for the silicon and germanium functional layers following the electron-selective contact were the same for both cells. The solar cells were finalized by a 300 nm thick $1 \times 1 \text{ cm}^2$ silver back contact, which was deposited via electron beam evaporation through a mask. After finalizing the deposition, the solar cells were annealed at 130°C in ambient air.

The external quantum efficiency (EQE) was recorded with an RR-2100 system from LOT Oriel. The current–voltage curves (J – V curves) were measured with a WACOM dual lamp solar simulator according to standard test conditions (AM1.5G spectrum, 1000 W m^{-2} , 25°C). Optical characterization was performed using a Cary 5000 spectrophotometer from Agilent with an integrating sphere. The transmittance of the solar cell layer stack was measured without the opaque back contact.

2.2. Electrical Modeling

The numerical software tool Afors-Het was used for electrical modeling.^[22] The parameters for the a-Si:H and a-Ge:H functional layers can be found in the work of Meddeb et al.,^[8] where the electrical model of the ultrathin a-Ge:H solar cell was introduced.

In the model, the n -doped silicon was substituted by a TiO_x layer and the corresponding parameters can be found in **Table 2**. For the simulations, an electron affinity (E_a) between 3.6 and 4.4 eV and a donor doping (D_n) between 1×10^{16} and $1 \times 10^{20} \text{ cm}^{-3}$ were used to map the large variety of material properties for TiO_x from the literature.^[19–21]

2.3. Optical Modeling

The layer absorption was calculated for every layer of the solar cells with a n a-Si:H or a TiO_x electron-selective contact with the 1D transfer matrix method using the software package CODE/scout. The models and the refractive index of the layers in the solar cell were introduced in previous publications.^[5,8] The

Table 1. Process parameters of the AZO and the TiO_x deposition.

	Power [W]	Ar flow [sccm]	Oxygen partial pressure [10^{-5} mbar]	Process pressure [10^{-3} mbar]	Passes	Speed [m min^{-1}]
AZO	3000	400	–	4	34	1.3
TiO_x	1800	300	4	3.3	4	0.55

Table 2. Parameters of TiO_x for modeling in Afors-Het.

Material	TiO_x
Thickness [nm]	7
Dielectric constant	11.9
Electron affinity [eV]	3.6–4.4
Bandgap [eV]	3.4
Effective (E_c/E_v) density [cm^{-3}]	1×10^{22}
Electron mobility [$\text{cm}^2 \text{V}^{-1} \text{s}$]	5
Hole mobility [$\text{cm}^2 \text{V}^{-1} \text{s}$]	1
Hole concentration [cm^{-3}]	0
Doping concentration donor [cm^{-3}]	1×10^{16} – 1×10^{20}
Dangling bonds acceptor/donor [cm^3]	1×10^{17}
Urbach tails width V_b/C_b [eV]	0.03
Interface defects density [cm^{-2}]	2.7×10^7
Interface model	Drift\diffusion

refractive index of the TiO_x layer was generated from optical models, which were fitted to measure spectral reflectance and transmittance spectra of single layers on glass substrates. The OJL model and the dielectric background model were used, which are provided by the software.^[23] **Figure 1** shows a comparison of the refractive indices for n a-Si:H and TiO_x . It can be seen that the refractive index n of TiO_x is smaller compared to n a-Si:H in the whole measured wavelength range. Furthermore, the extinction coefficient k is smaller as well, which leads to reduced parasitic absorption in the window layer.

3. Results and Discussion

The layer structure of the two studied solar cell configurations is shown in **Figure 2a**. The first configuration uses an n -doped amorphous silicon layer, whereas the second configuration uses TiO_x -based electron selective window layers. In both configurations, electron-selective contacts are deposited directly on top of the AZO front contact. The remaining layers are the same for both configurations: the a-Ge:H absorber is sandwiched by the intrinsic silicon buffer layers (i a-Si:H and $i \mu\text{c-Si:H}$), a p -doped hydrogenated microcrystalline silicon contact ($p \mu\text{c-Si:H}$), and a silver back contact (Ag).

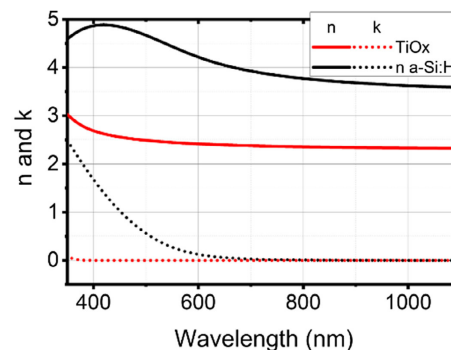


Figure 1. Refractive index and extinction coefficient of TiO_x and n a-Si:H.

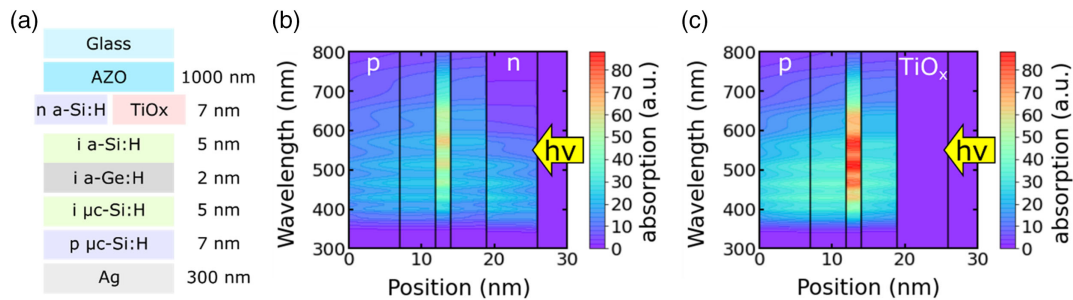


Figure 2. a) Layer stack of the a-Ge:H solar cells with *n* a-Si:H or TiO_x as electron-selective contact and the corresponding layer absorption plots with the integration of: b) *n* a-Si:H and c) TiO_x. The absorption is simulated with the 300 nm silver layer, which is not shown in the figure.

The calculated absorbance of the respective layers in two different configurations for the wavelengths ranging between 300 and 800 nm is shown in Figure 2b,c. The interference fringes in both figures are caused by the 1000 nm thick AZO front contact. The *n*-doped silicon absorbs mainly between 350 and 550 nm. It is known from the literature that light absorbed in doped layers contributes only to a very reduced extent to the photocurrent generation due to significant recombination.^[24,25] In contrast to that, the parasitic absorption of light in the TiO_x layer is very low due to its high bandgap. Also, below 350 nm almost no absorption occurs, because the light in this wavelength range is absorbed in the AZO front contact or the glass substrate, which is not shown in the figure. Furthermore, the absorption of light in the intrinsic layers including the nanoabsorber is much higher for the solar cell configuration using TiO_x as electron-selective contact. This effect can be attributed to the reduction of the absorption in the electron-selective contact. Light in the spectral range between 350 and 550 nm, which was previously absorbed in the window layer, is transmitted and absorbed in the intrinsic and *p*-doped layers instead. The absorption in the intrinsic layers is also improved due to the difference in the refractive index between the *n* a-Si:H and the TiO_x. Both layers are in contact with the AZO front contact layer in the respective configuration. Following Fresnel's law, the difference in the refractive index determines the value of the reflection coefficient. While small differences lead to lower reflection, large differences will lead to higher reflection. In the considered case, TiO_x has a refractive index of 2.4 at a wavelength of 550 nm, while the *n* a-Si:H has a

refractive index of 4.4. Compared to the refractive index of AZO, which is 1.8 at the same wavelength, the refractive index step at the interface is drastically reduced for TiO_x. Therefore, the reflection losses are lower. In addition, the refractive index of TiO_x is closer to that of silicon, so the boundary of the optical resonance cavity is effectively being moved from the *n* a-Si:H buffer/AZO interface to the *i* a-Si:H/TiO_x interface. Thus, the use of wide bandgap TiO_x as carrier selective contacts instead of *n* a-Si:H enables to reduce the optical nanocavity length and to minimize the parasitic absorption and reflection losses. This improves the effective absorption in the photoactive region and hence, enhances the photocurrent generation.

To validate our optical calculations, the external quantum efficiency (EQE) and the reflection *R* (presented as 1-*R*) of the two fabricated solar cells were measured (Figure 3a). It can be seen that the overall reflection is decreased for the solar cell with TiO_x compared to the solar cell with *n* a-Si:H. Therefore, the reflection losses are reduced and more light can be absorbed into the solar cell due to the TiO_x integration. Between 550 and 600 nm, the reflection was reduced up to 20%. This can be explained by the difference in the refractive index of TiO_x compared to *n* a-Si:H, as described earlier. The corresponding EQE curves show broadband absorption between 350 and 900 nm, which results in a photocurrent of 6.9 mA cm⁻² for both cells. As expected, an improved EQE is observed in the wavelength range between 350 and 500 nm for the solar cell with TiO_x in comparison to the solar cell with *n*-doped silicon. This indicates, that the parasitic absorption losses of blue light are successfully

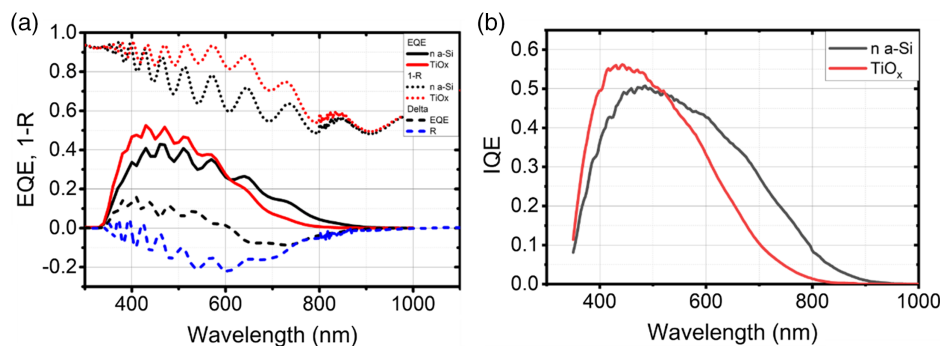


Figure 3. a) External quantum efficiency (EQE) and reflection *R* (presented as 1-*R*) and b) internal quantum efficiency (IQE) of the two fabricated solar cells with *n* a-Si:H or TiO_x as electron-selective contact.

reduced by integrating the TiO_x , since the EQE improvement in this wavelength range is higher than the reflection improvement. However, a decrease in the EQE occurs above 600 nm. A more detailed understanding can be obtained by calculating the internal quantum efficiency $\text{IQE} = \text{EQE}/(1-R)$. In Figure 3b, it can be seen that the IQE of the solar cell with TiO_x crosses the IQE of the solar cell with *n* a-Si:H at 530 nm. Hence, the parasitic absorption of blue light is reduced due to the integration of TiO_x . Furthermore, the expected improvement of the photocurrent generation for wavelengths larger than 530 nm due to the changed cavity length is negatively compensated by an effect, which is not considered in the optical simulations. The IQE shows a reduced absorption from the spectral position where the incident light is mainly absorbed in the a-Ge:H absorber according to the calculation in Figure 2. The substitution of the *n* a-Si:H layer with the TiO_x layer could have introduced detrimental changes in the layers subsequently deposited, i.e., a-Si:H buffer and a-Ge:H. An effect could be that the extraction of charge carriers from the quantum well is reduced. It has been shown in the literature that unintentional background doping in the barriers of quantum wells could reduce the carrier collection efficiency.^[26] Another explanation would be the induced recombination in the intrinsic layers due to higher defect densities. One source for the defects could be oxygen from the TiO_x , which reacted with the amorphous silicon. It has been shown in the literature that oxygen concentration above a critical contaminant level leads to detrimental solar cell performances in amorphous silicon solar cells and that the collection efficiency is reduced for increased oxygen concentrations.^[27,28] Furthermore, it is known from the literature that a mismatched atomic bond length in amorphous materials can lead to defect-rich interfaces. For example, it has been shown that materials like a-Si:H can have a defect-rich interfaces when they are grown on silicon nitride or silicon oxide substrates.^[29] Hence, the growth of the a-Si:H buffer in the solar cell with TiO_x could be defect rich. The Ti–O bond length is between 1.65 and 2.23 Å,^[30,31] and therefore significantly smaller bond length than a-Si:H with 2.34 Å.^[29] A reduced silicon quality can also adversely impact the a-Ge:H layer growth and hence the electrical properties of the solar cell. To investigate this further, *J–V* curves were recorded.

The *J–V* curves of the same solar cells are shown in Figure 4. The measured short circuit current J_{sc} for the two solar cells with

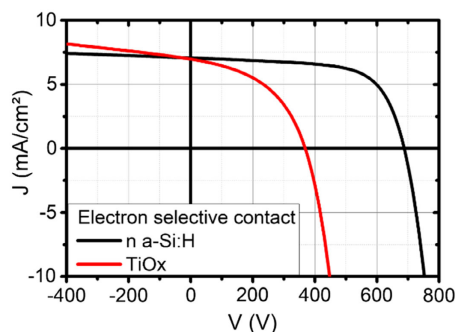


Figure 4. *J–V*-curves of the two solar cells with *n* a-Si:H and TiO_x electron-selective contacts.

n a-Si:H and TiO_x is between 7.1 and 7 mA cm^{−2} in good agreement with the value obtained from EQE. Furthermore, a diode behavior is observed and no s-shape due to electron blocking by a potential barrier at the TiO_x interface can be observed in the *J–V* curves. However, the solar cell with TiO_x has a lower open-circuit voltage (V_{oc}) of 368 mV and fill factor (FF) of 46% compared to the solar cell with *n* a-Si:H ($V_{\text{oc}} = 687$ mV, FF = 66%). The reduction of the V_{oc} agrees with the EQE, since the possible recombination losses leading to a reduced EQE for wavelengths >600 nm would lead also to a reduced saturation current. A reduction of the band gap in the germanium layer can be excluded by the EQE.

To further study the potential reason for the voltage loss and to outline a path to improve solar cell performance in the future, electrical modeling was performed. We vary the electron affinity in the range between 3.6 and 4.4 eV and the doping level from 1×10^{16} to 1×10^{20} cm^{−3} because both constitute crucial parameters for the performance of a solar cell.^[21,32] Figure 5 compares two band diagrams in equilibrium condition of two solar cells with *n* a-Si:H and TiO_x electron selective contact layer, respectively. It can be clearly seen that the shape of both band alignments is similar. In both cases, no barrier occurs at the interface between the electron-selective contact and the buffer, since the conduction band edge of the charge carrier-selective contact matches with the *i* a-Si:H conduction band. Furthermore, the conduction band offset at the *i* a-Si:H/*i* a-Ge:H interface is similar for both cases.

For a more detailed view, nine *J–V* curves were calculated for the different electron affinities and doping levels (see Figure 6). The curves show that for all configurations the V_{oc} is above 600 mV. Therefore, an inappropriate doping density or electron affinity is not the reason for the V_{oc} reduction of the measured solar cell with TiO_x . Interestingly, for all three doping levels, an s-shape occurs for an electron affinity of 4.4 eV, which was not observed in the measured *J–V* curves. For small electron affinities, the s-shape vanishes continuously with decreasing electron affinity. These results are in good agreement with calculations of TiO_x for silicon heterojunction technologies with a-Si passivation

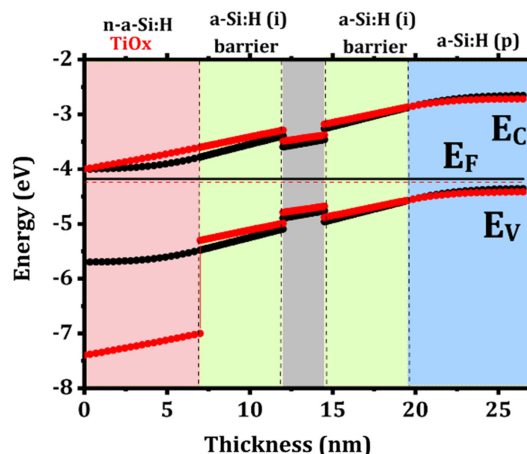


Figure 5. Comparison of the band diagrams for a solar cell with *n* a-Si:H (black line) and TiO_x (red line, $E_a = 4$ eV and $D_N = 1 \times 10^{18}$ cm^{−3}) electron-selective contact layer.

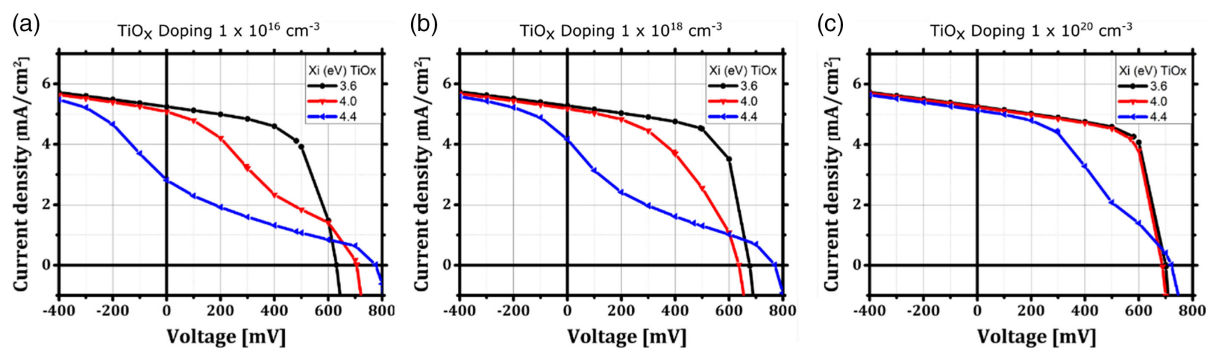


Figure 6. Simulated J - V curves for donor doping's of: a) 1×10^{16} , b) 1×10^{18} , c) 1×10^{20} , and electron affinities between 3.6 and 4.4 eV.

layers, which show that an electron affinity between 3.6 and 4.0 eV leads to the best solar cell performances.^[32] Furthermore, our calculations confirm that further optimization of the functional layers of the solar cell should allow an enhanced charge carrier extraction and therefore a higher V_{oc} . For further calculations, we used a donor doping of $1 \times 10^{18} \text{ cm}^{-3}$ and an electron affinity of 4 eV.

Apart from a possible band offset due to inappropriate choice of work function or doping, defects play an important role in the extraction of charge carriers. We found in our calculations that defects in the i a-Si:H buffer have the highest impact on the V_{oc} . Figure 7 shows calculated IV curves where the number of defects in the i a-Si:H buffer is continuously increased. It can be clearly seen that the V_{oc} is reduced from 550 to 400 mV. This could be explained due to shorter lifetimes of the charge carriers leading to enhanced recombination in the buffer layer. Furthermore, the simulated J_{sc} is also reduced for higher defect densities. This could explain why both fabricated solar cells have the same J_{sc} , also a higher photocurrent generation was expected for the solar cell with the TiO_x -based electron selective contact. This may be overcome by an optimization of the deposition process of the silicon buffer layer.

The TiO_x was not only integrated into the solar cell for enhancing the photocurrent generation, but also for increased transmittance in different applications like switchable solar cells and spectrally selective solar cells with transparent back contacts.

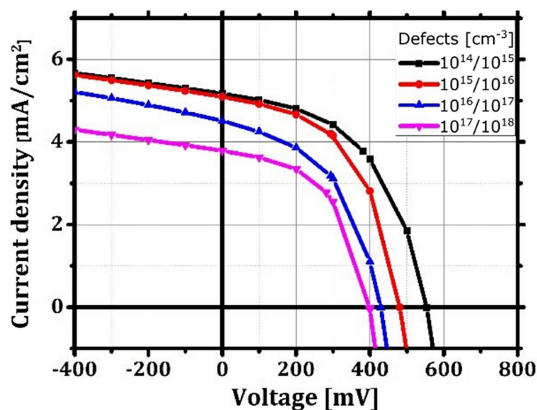


Figure 7. Calculated J - V curves for increased defect density in the tails/intermediate energy states of the a-Si:H buffer.

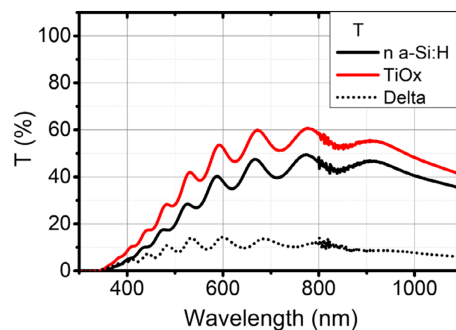


Figure 8. Transmission of the two solar cells measured between the silver back contacts.

Therefore, the transmittance of both fabricated solar cell layer stacks was measured without the silver back contacts shown in Figure 8. The solar cell layer stack with TiO_x as the window layer has a higher transmittance of light with wavelengths larger than 350 nm. The highest improvement of $\approx 15\%$ can be observed between 600 and 800 nm. Therefore, future integration of TiO_x into a-Ge:H solar cells for semitransparent applications could be promising.

4. Conclusion

In this work, we show that TiO_x is a suitable electron selective contact in an a-Ge:H solar cell with an absorber thickness of 2 nm. We observed an enhanced photocurrent generation for blue light and successful extraction of charge carriers was achieved. However, a reduction of the open-circuit voltage can be observed in comparison to an a-Ge:H solar cell with n -doped silicon as electron-selective contact. Our electrical calculations indicate that this is not caused by inappropriate electron affinity or TiO_x doping density, but rather due to induced defects in the i a-Si:H buffer. Hence, further interface engineering and an adaptation of the process parameters of the functional silicon and germanium layers deposited on the top of the TiO_x is needed to further improve the solar cell performance. Furthermore, the p -doped layer should be replaced in the future by other wide bandgap materials like molybdenum oxide for further reduction of parasitic absorption losses. Despite the electrical challenges we

also show that the TiO_x improves the transmittance of the solar cell. Therefore, TiO_x is a promising candidate to improve the a-Ge:H solar cell for semitransparent applications like switchable solar windows or spectrally selective solar cells for greenhouses.

Acknowledgements

The authors thank C. Lattayk, M. Götz-Köhler, and U. Banik for helpful discussion. This work was funded by the Energy branch of the German Aerospace Centre (DLR).

Open Access funding enabled and organized by Projekt DEAL.

Conflict of Interest

The authors declare no conflict of interest.

Data Availability Statement

The data that support the findings of this study are available from the corresponding author upon reasonable request.

Keywords

charge carrier-selective contacts, optoelectronic simulations, quantum wells, ultrathin amorphous germanium solar cells

Received: May 4, 2022

Revised: July 20, 2022

Published online: August 19, 2022

- [1] M. Götz, M. Lengert, N. Osterthun, K. Gehrke, M. Vehse, C. Agert, *ACS Photonics* **2020**, *7*, 1022.
- [2] C. J. Traverse, R. Pandey, M. C. Barr, R. R. Lunt, *Nat. Energy* **2017**, *2*, 849.
- [3] K. Lee, H.-D. Um, D. Choi, J. Park, N. Kim, H. Kim, K. Seo, *Cell Rep. Phys. Sci.* **2020**, *1*, 100143.
- [4] M. Götz, N. Osterthun, K. Gehrke, M. Vehse, C. Agert, *Coatings* **2020**, *10*, 218.
- [5] N. Osterthun, N. Neugebohrn, K. Gehrke, M. Vehse, C. Agert, *Opt. Express* **2021**, *29*, 938.
- [6] H. Shi, R. Xia, G. Zhang, H.-L. Yip, Y. Cao, *Adv. Mater.* **2019**, *9*, 1803438.
- [7] V. Steenhoff, M. Juilfs, R.-E. Ravekes, M. Ahrlich, M. Kellermann, O. Siepman, M. Vehse, C. Agert, *IEEE J. Photovolt.* **2017**, *7*, 3.
- [8] H. Meddeb, N. Osterthun, M. Götz, O. Sergeev, K. Gehrke, M. Vehse, C. Agert, *Nano Energy* **2020**, *76*, 105048.
- [9] H. Meddeb, N. Osterthun, M. Götz, O. Sergeev, K. Gehrke, M. Vehse, C. Agert, presented at *47th IEEE Photovolt. Spec. Conf.*, Calgary, AB, Canada **2020**.
- [10] E. G. Barbagiovanni, D. J. Lockwood, P. J. Simpson, L. V. Goncharova, *J. Appl. Phys.* **2012**, *111*, 034307.
- [11] J. Parravicini, F. D. Trapani, M. D. Nelson, Z. T. Rex, R. D. Beiter, T. Catelani, M. F. Acciarri, A. Podesta, C. Lenardi, S. O. Binetti, *ACS Appl. Nano Mater.* **2020**, *3*, 2813.
- [12] T. G. Allen, J. Bullock, X. Yang, A. Javey, S. De Wolf, *Nat. Energy* **2019**, *4*, 914.
- [13] P. Gao, Z. Yang, J. He, J. Yu, P. Liu, J. Zhu, Z. Ge, J. Ye, *Adv. Sci.* **2018**, *5*, 1700547.
- [14] J. Tournet, J. D. Butson, P. R. Narangari, S. Dontu, B. Gupta, M. Lysevych, S. Karuturi, H. H. Tan, C. Jagadish, *Phys. Status Solidi RRL* **2021**, *15*, 2100282.
- [15] T. Matsui, M. Bivour, P. Ndione, P. Hettich, M. Hermle, *Energy Proc.* **2017**, *124*, 628.
- [16] T. Matsui, M. Bivour, P. F. Ndione, R. S. Bonilla, M. Hermle, *Sol. Energy Mater. Sol. Cells* **2020**, *209*, 110461.
- [17] M. Mirsafaei, P. B. Jensen, M. Ahmadpour, H. Lakhotiya, J. L. Hansen, B. Julsgaard, H.-G. Rubahn, R. Lazzari, N. Witkowski, P. Balling, M. Madsen, *ACS Appl. Energy Mater.* **2019**, *3*, 253.
- [18] V. Titova, J. Schmidt, *Phys. Status Solidi RRL* **2021**, *15*, 2100246.
- [19] X. Yin, C. Battaglia, Y. Lin, K. Chen, M. Hettick, M. Zheng, C. Y. Chen, D. Kiriya, A. Javey, *ACS Photonics* **2014**, *1*, 1245.
- [20] J. Bullock, Y. Wan, M. Hettick, X. Zhaoran, S. P. Phang, D. Yan, H. Wang, W. Ji, C. Samundsett, Z. Hameiri, D. Macdonald, A. Cuevas, A. Javey, *Adv. Mater.* **2019**, *9*, 1803367.
- [21] M. C. K. Sellers, E. G. Seebauer, *Thin Solid Films* **2011**, *519*, 2103.
- [22] R. Varache, C. Leendertz, M. Gueunier-Farret, J. Haschke, D. Muñoz, L. Korte, *Sol. Energy Mater. Sol. Cells* **2015**, *141*, 14.
- [23] S. K. O'Leary, S. Johnson, P. Lim, *J. Appl. Phys.* **1997**, *82*, 3334.
- [24] N. Jensen, U. Rau, R. M. Hausner, S. Uppal, L. Oberbeck, R. B. Bergmann, J. H. Werner, *J. Appl. Phys.* **2000**, *87*, 2639.
- [25] Z. C. Holman, A. Descoedres, L. Barraud, F. Z. Fernandez, J. P. Seif, S. De Wolf, C. Ballif, *IEEE J. Photovolt.* **2012**, *2*, 7.
- [26] K. Toprasertpong, T. Inoue, Y. Nakano, M. Sugiyama, *Sol. Energy Mater. Sol. Cells* **2018**, *174*, 146.
- [27] J. Woerdenweber, T. Merdzhanova, R. Schmitz, A. Mück, U. Zastrow, L. Niessen, A. Gordijn, R. Carius, W. Beyer, H. Stiebig, U. Rau, *J. Appl. Phys.* **2008**, *104*, 094507.
- [28] M. Isomura, T. Kinoshita, Y. Hishikawa, S. Tsuda, *Appl. Phys. Lett.* **1994**, *65*, 2329.
- [29] B. Abeles, T. Tiedje, *Phys. Rev. Lett.* **1983**, *51*, 2003.
- [30] K. Kaur, S. Prakash, N. Goyal, *J. Mater. Res.* **2011**, *26*, 2604.
- [31] H.-Y. Lee, S. J. Clark, J. Robertson, *Phys. Rev. B* **2012**, *86*, 075209.
- [32] H. Mehmood, H. Nasser, T. Tauqeer, R. Turan, *Renew. Energy* **2019**, *143*, 359.